Pyrolysis of *Camellia oleifera* Shell at Intermediate Temperatures, and Prediction of Bio-oil Component Levels by Mathematical Modeling

Rongqu Bei,[a] Wenrui Xie,[b] Xuefei Gan,[a,*] Yuefang Chen,[a] and Zhengbin He [b,*]

Camellia oleifera shell was pyrolysed at 300 to 750 °C to investigate biochar and bio-oil yields under different conditions, and the relationships between pyrolysis temperature and the product yields were established. The thermal decomposition behavior, biochar characteristics, and bio-oil composition were analyzed. The fixed carbon content of *C. oleifera* shell reached 22.2%, exceeding common biomass materials. Biochar yield decreased from 57.9% to 31.7% as temperature increased from 300 °C to 750 °C, while bio-oil yield increased from 14.4% to 37.1%. The established temperature-dependent yield models demonstrated excellent predictive capability (R^2=0.99). Final carbonization levels under heating rates of 5, 10, and 15 °C/min were 35.4%, 29.4%, and 27.2%, respectively. Biochar pore volume increased with pyrolysis temperature, while specific surface area and average pore diameter exhibited an initial rise followed by decline. Specific surface area increased as temperature rose, with predominant pore diameters distributed between 10 and 30 nm. Bio-oil composition analysis revealed acids as predominant components (40.9% to 49.9%), followed by phenols (20.2% to 27.3%), aldehydes (9.2% to 10.2%), ketones (8.4% to 11.8%), esters (3.4% to 3.6%), and alcohols (0.41% to 1.07%). This study provides guidance for optimizing pyrolysis conditions to obtain target products.

DOI: 10.15376/biores.20.4.10893-10905

Keywords: Pyrolysis characteristics; Model construction; TG; GC-MS; BET

Contact information: a: Wuzhou Forestry Science Research Institute, Wuzhou Engineering Technology Research Center for High-Yield Cultivation of Camellia oleifera 'Soft Branch', No. 14, Xinxing Zhubao Road, Changzhou District, Wuzhou, Guangxi 543002, PR China; b: State Key Laboratory of Efficient Production of Forest Resources, Beijing Key Laboratory of Wood Science and Engineering, MOE Key Laboratory of Wooden Material Science and Application, College of Material Science and Technology, Beijing Forestry University, No. 35, Qinghua Eastroad, Haidian District, Beijing 100083, PR China;
** Corresponding author: 996322127@qq.com and hzbcailiao@bjfu.edu.cn*

INTRODUCTION

Camellia oleifera shell is the primary byproduct generated during the processing of *C. oleifera* fruits. As the world's largest cultivator of *C. oleifera*, China possesses abundant reserves of this lignocellulosic residue. According to the data from the China Statistical Yearbook, by the end of 2023, the total planting area of *C. oleifera* in China had reached approximately 4.87 million hectares, and the annual yield of *C. oleifera* seeds was approximately 3.37 million tons. Given that the shell constitutes 50% to 60% of the total seed mass, over 1.68 million metric tons of *C. oleifera* shells are produced annually (Xia *et al.* 2021; Zheng *et al*. 2024). *C. oleifera* shell exhibits high carbon, hydrogen, and oxygen content, coupled with elevated fixed-carbon content and calorific value, positioning it as a

valuable resource with significant development potential (Meng *et al.* 2022).

Currently, *C. oleifera* shell are treated by incineration, composting, landfilling, and thermal treatment. However, incineration generates substantial CO_2 emissions and particulate matter, composting suffers from extended cycles and low efficiency, while landfilling poses risks of leachate contamination and land occupation (Zhang *et al.* 2018).

Pyrolysis has emerged as a promising thermochemical conversion technology due to its efficiency and environmental compatibility. This oxygen-deprived thermal degradation process could convert *C. oleifera* shells into value-added products (biochar, bio-oil, syngas) through complete resource utilization (Zhang *et al.* 2015; Zhang *et al.* 2016; Chen *et al.* 2018; Liu *et al.* 2022). Biochar, containing porous carbon, and could be used in soil amendment and pollutant adsorption. Bio-oil rich in phenolic compounds, ketones, and carboxylic acids shows potential for fuel upgrading, chemical extraction, and agricultural utilization. Syngas comprising CO, H_2, and CH_4 serves as feedstock for power generation and synthetic gas production (Mehmood *et al.* 2022; Yuan *et al.* 2022; Tang *et al.* 2024). Current research on *C. oleifera* shell has focused on the extraction of functional components, material utilization, fertilizer production, and energy conversion, *etc*. The pyrolysis of *C. oleifera* shell concentrates on the influence of treatment conditions on the yield of products, the characteristics of products, and pyrolysis kinetics (Xu and Jiang 2014; Xiao *et al.* 2022; Xu *et al.* 2022a; Zhang *et al.* 2025).

Although the general trends of pyrolysis experiments are largely consistent, differences still exist due to the nonlinear nature of product conversion. Therefore, accurately predicting the variation of pyrolysis product yields with operating conditions is crucial for process optimization and design. Constructing mathematical models, either in empirical or analytical form, to characterize the relationship between yields and process parameters provides a theoretical basis for optimizing operating parameters and feedstock selection. By applying response surface methodology (RSM) to fit quadratic polynomials, it is possible to establish quadratic polynomial models of bio-oil yield based on multiple factors such as final pyrolysis temperature, nitrogen flow rate, and heating rate (Fan *et al*. 2014; Dai *et al*. 2020). The distributed activation energy model (DAEM) has also been widely employed to analyze the pyrolysis characteristics and volatile compositions of various materials, including *C. oleifera* shells (Yang *et al*. 2019). In addition, simple polynomial/least-squares regression is frequently used to construct the relationships between the yields of products such as biochar and bio-oil and the pyrolysis temperature (Papuga *et al*. 2024; Awad *et al*. 2024).

Although previous studies have applied mathematical models to fit the relationships between pyrolysis product yields and pyrolysis conditions, very few reports have focused on developing yield prediction models specifically for *C. oleifera* shell pyrolysis. Moreover, a lack of external validation against independent experimental data has limited the ability to reliably evaluate the accuracy of these models. In this paper, the characteristics of pyrolysis products of *C. oleifera* shell under different heat treatment conditions was studied by use of thermogravimetry (TG), gas chromatography-mass spectrometry (GC-MS) and the Brunauer-Emmet-Teller (BET) method of surface area analysis. A model describing the relationship between pyrolysis temperature and product yields was established and further validated by independent experiments, laying a foundation for the regulation of pyrolysis process of *C. oleifera* shell and the utilization of these products.

EXPERIMENTAL

C. oleifera shells were collected from Wuzhou, Guangxi Province, China. The moisture, ash, volatile matter, and fixed carbon contents of *C. oleifera* shells were determined by proximate analysis. The elemental composition (C, H, N, S) was quantified by ultimate analysis, and the oxygen content was calculated by mass difference. Pyrolysis was conducted at 300, 450, 600, or 750 °C. To ensure complete pyrolysis and stable product properties, the residence time was set to 2 h (Sun *et al.* 2016). Biochar and bio-oil yields were quantified, and the predictive models were established *via* multivariate regression analysis. Thermogravimetric analysis coupled with Fourier transform infrared spectroscopy (TG-FTIR, Netzsch STA 2500 (Germany)/Thermo Fisher IS50 (USA)) was used to investigate the effects of heating rates (5, 10, 15 °C/min) on the thermal decomposition characteristics of *C. oleifera* shells within the temperature range of 30 to 900 °C, as well as the functional group evolution and release profiles of pyrolysis gas components during the pyrolysis process. The specific surface area and pore size distribution of the biochar were investigated using a fully automated BET analyzer (Micromeritics ASAP 2460, USA) through N_2 adsorption-desorption. The composition and relative content of bio-oil were analyzed by GC-MS (Shimadzu LC-20A, Japan), with the obtained spectra matched against the NIST2011 standard library, retaining only organic compounds with a similarity index (IS) greater than 80% and a relative content above 0.1%.

RESULTS AND DISCUSSION

Proximate and Elemental Analysis

The proximate and ultimate analysis results of *C. oleifera* shell are shown in Table 1. The proximate analysis indicated that the ash content of the shell was relatively low at 2.79%, while the fixed carbon content was 22.15%, which is higher than that of common biomass materials such as moso bamboo, rice straw, and Scots pine. The ultimate analysis reveals that the main elemental composition of the shell was C, H, and O, with the combined content of these three elements exceeding 95%.

Table 1. The Proximate and Ultimate Analysis Results of *C. oleifera* Shell

Proximate analysis (%)				Elemental analysis (%)				
moisture	ash	volatile matter	fixed carbon	C	H	O*	N	S
0.77	2.79	74.29	22.15	46.46	5.75	47.345	0.445	0

Note: * by mass difference

Pyrolysis Characteristics and Model Construction

Effect of pyrolysis temperatures and temperature ramping rates on pyrolysis products

Table 2 presents the yields of bio-oil and biochar from *C. oleifera* shells under different pyrolysis temperatures and temperature ramping rates. As shown in the table, the biochar yield decreased from 57.9% to 31.7% with increasing temperature, which can be attributed to the primary decomposition of cellulose, hemicellulose, and lignin at lower temperatures, which generated solid biochar and a small amount of volatiles. As the temperature increased, the organic components in the biochar further decomposed, producing more gaseous and liquid products, thereby reducing the mass of solid biochar.

Concurrently, the bio-oil yield increased from 14.4% to 37.1% with rising temperature. This was mainly because the pyrolysis reactions of cellulose, hemicellulose, and lignin intensified, generating more volatiles (such as organic acids, phenols, and aldehydes), which condensed to form bio-oil (Yang *et al.* 2007).

Table 2. The Yields of Bio-Oil and Biochar for *C. oleifera* Shells Under Different Pyrolysis Conditions

Temperature (°C)	Raw Material Weight (g)	Biochar Weight (g)	Bio-oil Weight (g)	Biochar Yield per Unit Mass (%)	Bio-oil Yield per Unit Mass (%)
300	155.00	89.71	22.37	57.88	14.43
450	161.29	70.46	44.16	43.69	27.38
600	155.37	52.30	56.08	33.66	36.09
750	158.23	50.16	58.66	31.70	37.07

Relationship models between bio-oil/biochar yields and thermal treatment temperature

To better utilize the pyrolysis products of *C. oleifera* shells and predict the yields of bio-oil and biochar under different pyrolysis temperatures, relationship models between pyrolysis temperature and product yields were established. The four sets of yield data for biochar and bio-oil were imported into TableCurve 3D, respectively. This software contains a library of many thousands of equations, from which it picks those that achieve the best fits to the data with relatively few terms. For biochar, the yield prediction model was selected as the function ranked second in fitting performance, with a Fitting Standard Error (FSE) of 0.038; for bio-oil, the yield prediction model was selected as the function ranked first, with an FSE of 0.005. A smaller FSE value indicates a better fit of the curve to the data. Meanwhile, the R^2 values of both models were 0.99, indicating excellent fitting performance and the ability to accurately predict biochar and bio-oil yields under varying pyrolysis temperatures. These models provide robust theoretical support for optimizing the pyrolysis process of *C. oleifera* shells. Equation 1 describes the relationship between biochar yield and treatment temperature, while Eq. 2 represents the relationship between bio-oil yield and treatment temperature, as follows,

$$m_1 = 82.53 - 54.58\times10^{-4}\cdot t^{\frac{3}{2}} + 1.45\times10^{-7}t^3 \quad R^2=0.99 \tag{1}$$

$$m_2 = (-37.06\times10^{-3} + 5.52\times10^{-5}\cdot t + \frac{465.4}{t^{\frac{3}{2}}})^{-1} \quad R^2=0.99 \tag{2}$$

where m_1 represents the biochar yield per unit mass of raw material (%), m_2 denotes the bio-oil yield per unit mass of raw material (%), and t is the thermal treatment temperature (°C).

To verify the accuracy of the model, an intermediate temperature of 525 °C, which is between 450 and 600 °C, was selected as the verification temperature, with the pyrolysis feedstock weight of *C. oleifera* shells being 160.67 g. The biochar and bio-oil yields at 525 °C were simultaneously substituted into Eq. 1 and Eq. 2, and the predicted results were compared with the experimental values to calculate the accuracy of this model. The error was determined using the following Eq. 3:

$$E = \frac{P_0 - P}{P} \times 100\% \tag{3}$$

where E represents the error, P_0 is the predicted value, and P is the experimental value. The

comparison between predicted and experimental data of the biochar and bio-oil yields are presented in Table 3. It can be observed that the errors of both the biochar and bio-oil yields prediction models are less than 5%, confirming the reliable predictive capability of the models.

Table 3. Comparison between Predicted and Experimental Data of the Biochar and Bio-oil Yields

Raw material type	Product Yield per Unit Mass of Raw Material (%)	Predicted product Yield per Unit Mass of Raw Material (%)	Error (%)
Biochar	36.24	37.86	4.45
Bio-oil	31.42	32.67	3.98

Thermodynamic Analysis of *Camellia oleifera* Shell (TG)

Thermogravimetric analysis (TG) measures the relationship between the thermal degradation process of the sample and the treated time, and derivative thermogravimetry (DTG) reflects the rate of weight loss during pyrolysis. Figure 1 presents the TG and DTG curves of *C. oleifera* shells decomposed at the heating rates of 5, 10, and 15 °C/min. It can be observed that the mass of the *C. oleifera* shell sample decreased with increasing temperature. Based on the weight loss rates, the TG curve can be roughly divided into three stages: moisture evaporation, pyrolysis, and carbonization (Meng *et al.* 2022).

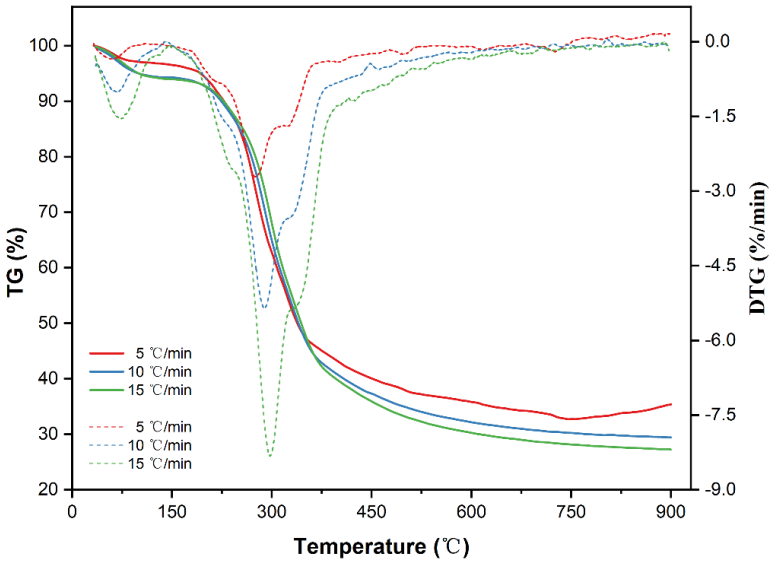

Fig. 1. TG-DTG curve of *C. oleifera* shell

The DTG curve revealed a rapid weight loss stage before 100 °C, attributed to moisture evaporation. Subsequently, the weight loss rate slowed down between 100 to 220 °C, during which bound water was gradually released, and hemicellulose and lignin began to decompose. A distinct weight loss peak appeared at the 220 to 380 °C stage, indicating intensified decomposition of hemicellulose, along with significant degradation of cellulose and lignin. Hemicellulose, with its abundant side chains, exhibits poor thermal stability and is highly sensitive to heat treatment. At relatively low temperatures, these side chains easily break down, producing organic and gaseous products such as alcohols, aldehydes, CO, and

CO_2. Simultaneously, the main chains of xylan in hemicellulose also undergo depolymerization, with D-xylose monomers decomposing to acids, aldehydes, and alcohols. Lignin, with its complex structure, primarily generates phenolic compounds during pyrolysis (Zhang *et al.* 2022). As temperatures continue to rise, the DTG curve stabilized, and the sample lost weight, but the weight loss rate was relatively slow. During this stage, lignin undergoes a series of complex free-radical recombination processes, including cleavage of the phenylpropane side chains, dealkylation, demethylation, dehydration, and dehydrogenation (Carrier *et al*. 2017). These reactions increase the degree of molecular crosslinking, resulting in highly aromatized lignin with a more stable aromatic ring skeleton. Meanwhile, certain lignin-derived intermediates, such as phenols and light tars, are adsorbed onto the char surface and undergo secondary reactions through polymerization, together with the original char, forming polycyclic aromatic structures with a higher degree of polymerization (Keiluweit *et al*. 2010; Liu *et al*. 2008). The final carbonization yields of *C. oleifera* shells at heating rates of 5, 10, and 15 °C/min were 35.4%, 29.4%, and 27.2%, respectively.

TG-FTIR Analysis

Thermogravimetric analysis coupled with Fourier transform infrared spectroscopy (TG-FTIR) was used to determine the characteristics of gaseous products during the heating process. The TG-FTIR spectra of *C. oleifera* shells at three heating rates (5, 10, and 15 °C/min) are shown in Fig. 2 (a, b, and c, respectively). At different heating rates, the gas release peaks were at 279.7 °C, 293.1 °C, and 304.5 °C, respectively.

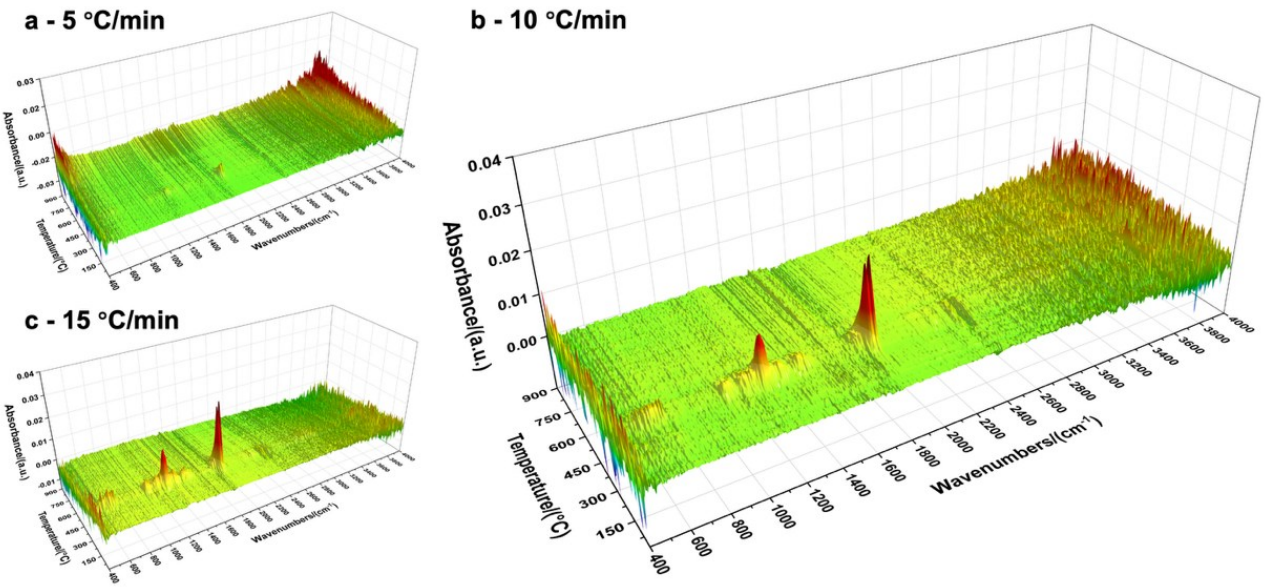

Fig. 2. TG-FTIR curves of *C. oleifera* shells (a: 5 °C/min, b: 10 °C/min, c: 15 °C/min)

Figure 3 shows the FTIR spectra corresponding to the absorbance peaks observed at the three heating rates. Peaks in the range of 3400 to 4000 cm^{-1} appeared in all three heating rate conditions, representing the stretching vibration of -OH, corresponding to water or alcohols (Xu *et al.* 2022b). Water is primarily generated through the cleavage of aliphatic hydroxyl groups in the side chains, intramolecular and intermolecular crosslinking reactions of glucose, and dehydroxylation of cellulose and hemicellulose. Free water is released from *C. oleifera* shells (before 100 °C), and other water molecules are

produced through condensation and polycondensation reactions of intermediate products (after 100 °C) during pyrolysis. Alcohols are formed due to the cleavage of O-methyl groups at the C4 position of glucuronic acid units or methyl groups in lignin (Yang *et al.* 2007; He *et al.* 2019). The peaks in the range of 2700 to 3000 cm^{-1} correspond to the stretching vibration of C-H bonds, indicating the presence of methyl (-CH_3) and methylene (-CH_2-) groups, with CH_4 as the representative compound (Liu *et al.* 2008). The absorbance peak around 2380 cm^{-1} represents the stretching vibration of C=O, corresponding to the release of CO_2, which is mainly generated through decarboxylation of carbonyl groups, decomposition of dehydrocellulose, or decarboxylation of -COOH groups in glucuronic acid units. It may also result from the cleavage and recombination of C=O and -COOH groups, decarboxylation of O-acetyl groups linked to xylan, or cleavage of acetyl and carbonyl groups on the xylan chain of hemicellulose. The absorbance peaks around 2000 to 2250 cm^{-1} correspond to the weak characteristic absorbance of CO, which is more pronounced at a heating rate of 15 °C/min but less noticeable in the other two groups. The peak around 1798 cm^{-1} also represents the stretching vibration of C=O, possibly corresponding to aldehydes, ketones, or acids, while the peaks around 1173 to 1183 cm^{-1} represent the stretching vibration of C-O, corresponding to alcohols, esters, and ethers. The C=O stretching vibration may correspond to compounds such as 3-furaldehyde and acetic acid, while the C-O stretching vibration may correspond to alcohols and esters produced during the pyrolysis of cellulose or hemicellulose in *C. oleifera* shells (Tong *et al.* 2014).

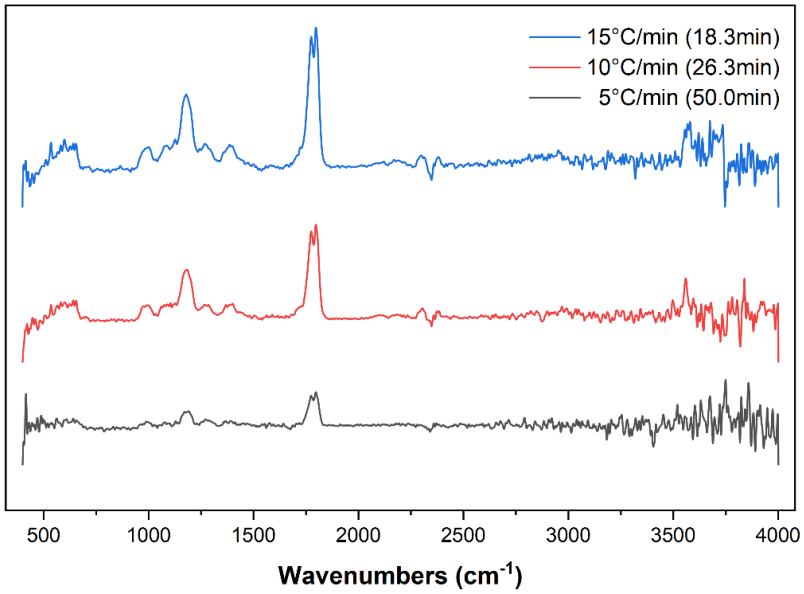

Fig. 3. FTIR spectra of *C. oleifera* shells at three heating rates

Figure 4 illustrates the variation in concentration of gaseous products from *C. oleifera* shells over time at three heating rates. According to the Beer-Lambert law, the gas concentration is proportional to the absorbance under constant optical conditions, and thus the changes in absorbance curves reflect the concentration trends of the substances during pyrolysis (He *et al.* 2018). The concentration of -OH remains at a high level under all three heating rates. At 290 °C, the concentrations of C-O and C=O increased greatly, surpassing that of –OH group. The curves corresponding to faster heating rates exhibit notably higher peak absorbances for -OH and C=O, indicating higher yields of gaseous products.

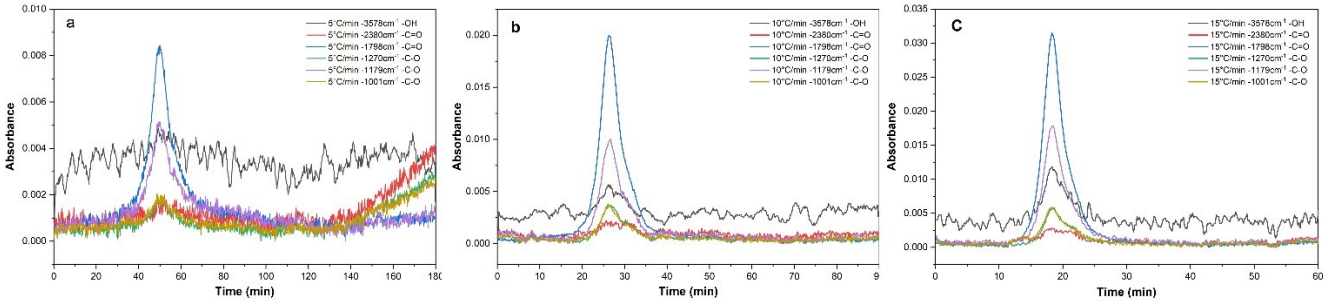

Fig. 4. The variation in concentration of gaseous products from *C. oleifera* shells over time at three heating rates (a: 5 °C/min, b: 10 °C/min, c: 15 °C/min)

BET Analysis of Biochar

To investigate the pore structure of biochar derived from *C. oleifera* shells during pyrolysis, Table 4 presents the specific surface area, pore size, and pore volume of biochar at different pyrolysis temperatures. The average pore volume of the samples increased with increasing temperature. The specific surface area and average pore size of the samples initially increased and then decreased with increasing temperature. The specific surface area of the samples treated at 600 and 750 °C was larger than that at 450 °C, while the average pore size of the sample at 750 °C was smaller than the other two groups. The main components of *C. oleifera* shells decomposed at high temperatures, releasing volatile substances. As the temperature increases, these volatiles escape, leaving open fibrous structures and cavities in the carbon (Shrivastava *et al.* 2021). Higher pyrolysis temperatures intensified the release of volatiles, leading to increased average pore volume. When the pyrolysis temperature rose from 450 to 600 °C, both the specific surface area and average pore size of the samples increased, with the specific surface area increasing from 0.98 to 1.96 m^2/g. This result shows that lower pyrolysis temperatures may cause the condensation of volatiles, blocking pores and resulting in a lower specific surface area (Biswas *et al.* 2024). At higher temperatures, lignin undergoes pyrolysis, forming more stable carbon. Lignin pyrolyzes over a wide temperature range, primarily between 500 to 600 °C. The complex three-dimensional network structure of lignin undergoes condensation reactions of free radicals and aromatic rings, forming aromatic compounds and ultimately stable carbon structures (Miao *et al.* 2025). Therefore, the pyrolysis of the main components in *C. oleifera* shells was essentially completed at 600 °C. At 750 °C, the specific surface area and average pore size of the samples decreased, which was likely due to the melting of low-melting-point ash and tar blocking some pores, or structural changes such as pore collapse (Chen *et al.* 2014).

Table 4. Specific Surface Area, Pore Volume and Pore Size of *C. oleifera* Shell Biochar at Different Pyrolysis Temperatures

Temperature (°C)	Specific surface area (m^2/g)	Pore volume (cm^3/g)	Pore size (nm)
450	0.98	0.002976	26.8742
600	1.96	0.004037	27.5074
750	1.84	0.004788	21.8314

The N_2 adsorption-desorption isotherms and pore size distribution curves are shown in Fig. 5. The isotherms of the biochar at the three pyrolysis temperatures are similar, and

most of the pore sizes were distributed between 10 to 30 nm. According to the International Union of Pure and Applied Chemistry (IUPAC) classification, pores are divided into macropores (> 50 nm), mesopores (2 to 50 nm), and micropores (< 2 nm). In the low-pressure region ($P/P_0 < 0.2$), the adsorption curve shows a slight upward trend, indicating micropore adsorption. The sample at 600 °C exhibits stronger adsorption in this region, suggesting a more abundant mesoporous structure compared to the other two groups. Subsequently ($P/P_0 = 0.2$ to 0.7), the curve enters an adsorption plateau. Finally, in the high-pressure region ($P/P_0 > 0.7$), the adsorption curve increases sharply, and the isotherm does not reach a plateau, indicating that adsorption is not saturated.

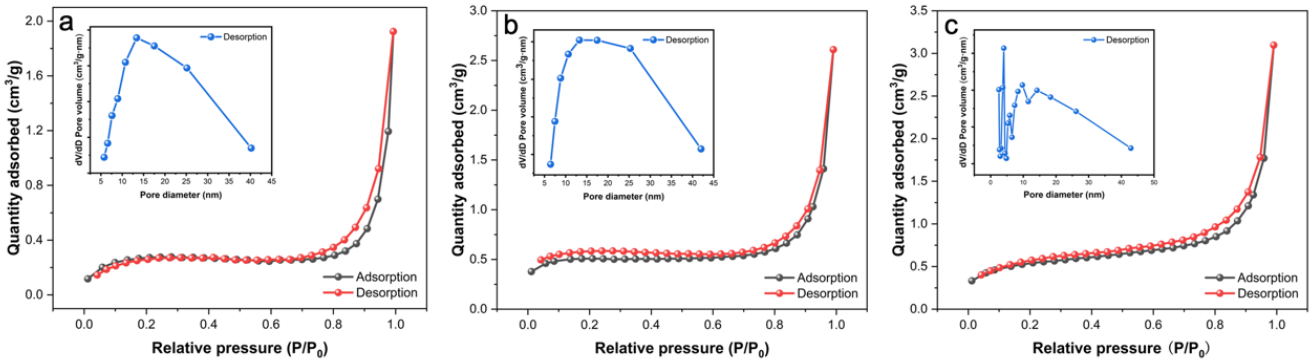

Fig. 5. N_2 adsorption-desorption isotherms and pore size distribution of *C. oleifera* shell carbon at different pyrolysis temperatures (a: 450 °C, b: 600 °C, c: 750 °C)

GC-MS Analysis

To determine the composition and content of bio-oil generated from the pyrolysis of *C. oleifera* shells and investigate the effects of different pyrolysis temperatures on bio-oil composition and content, GC-MS analysis was performed on bio-oil samples obtained at pyrolysis temperatures of 450, 600, and 750 °C. The main components and their relative contents in bio-oil at different pyrolysis temperatures are shown in Table 5.

Table 5. Bio-oil Contents (%) at Different Pyrolysis Temperatures

Component(%)	Pyrolysis Temperature (°C)		
	450	600	750
Acids	49.86	41.42	40.92
Esters	3.35	4.1	3.64
Aldehydes	9.17	8.69	10.25
Ketones	8.37	11.46	11.76
Phenols	20.24	30.18	27.34
Alcohols	1.07	1.34	0.41
Other substances	7.94	2.81	5.68

Excluding water, acids were the most abundant components in bio-oil. The relative content of acids decreased with increasing pyrolysis temperature, while the relative content of phenols initially increased and then decreased, peaking at 600 °C. The relative contents of aldehydes and ketones were similar, with the content of ketones increasing with pyrolysis temperature. Therefore, adopting a lower pyrolysis temperature (*e.g.*, 450 °C) can increase the proportion of acidic substances in bio-oil, which, when applied to soil modification, can more effectively reduce soil pH. In contrast, bio-oil produced at a higher pyrolysis temperature (*e.g.*, 600 °C) contained a higher content of phenolic compounds,

which can effectively suppress soil pathogens and enhance soil biodiversity when applied to soil (Stutz *et al*. 2017).

FUTURE WORK

1. In future work, the variables of the yield prediction model could be extended from a single temperature factor to multiple variables, such as different heating rates, residence times, and particle sizes, thereby providing a more reliable predictive tool for process refinement and control.
2. In future studies, liquid chromatography-mass spectrometry (LC-MS) could be employed to analyze the components of bio-oil, which would avoid the influence of extraction steps on result accuracy and overcome the limitation that certain compounds cannot be vaporized within the temperature range of GC-MS, thus making them difficult to detect.

CONCLUSIONS

1. The gas release peaks of *C. oleifera* shells appeared at 279.7, 293.1, and 304.5 °C under heating rates of 5, 10, and 15 °C/min, respectively. With the increase of heating rate, the relative content of functional group components corresponding to medium absorbance (represented by bio-oil) gradually increased, and at the maximum heating rate, the release peaks were concentrated within a relatively narrow temperature range.
2. A temperature–yield prediction model for the pyrolysis of *C. oleifera* shells was established and validated, showing a high coefficient of determination ($R^2 = 0.99$). This model accurately predicted the yields of biochar and bio-oil under different temperature treatments, thereby providing a theoretical tool for optimizing pyrolysis processes.
3. As the temperature increased from 300 to 750 °C, the biochar yield of *C. oleifera* shells decreased from 57.9% to 31.7%, while the bio-oil yield increased from 14.4% to 37.1%. The bio-oil was dominated by acids (approximately 41–50%), and the phenolic content reached its maximum at 600 °C, indicating that the pH value and phenolic content of bio-oil can be tuned by selecting appropriate pyrolysis temperatures.
4. With increasing pyrolysis temperature, the average pore volume of biochar increased, while the specific surface area rose from 0.98 m^2/g at 450 °C to 1.96 m^2/g at 600 °C, and slightly decreased to 1.84 m^2/g at 750 °C. The pore size was mainly distributed in the range of 22 to 27 nm, suggesting that medium-to-high pyrolysis temperatures favor the formation of mesoporous structures with adsorption capacity, whereas excessively high temperatures may lead to pore blockage or collapse.

ACKNOWLEDGMENTS

This work was supported by Guangxi Specialized Funding Project for Science and Technology Base and Talent (Guike AD23049004) and Science and Technology Program of Inner Mongolia Autonomous Region (2025KYPT0175).

REFERENCES CITED

Awad, M., Makkawi, Y., and Hassan, N. (2024). "Yield and energy modeling for biochar and bio-oil using pyrolysis temperature and biomass constituents," *ACS Omega* 9(16), 18654-18667. DOI: 10.1021/acsomega.4c01646

Biswas, B., Balla, P., Krishna, B., Adhikari, S., and Bhaskar, T. (2024). "Physiochemical characteristics of bio-char derived from pyrolysis of rice straw under different temperatures," *Biomass Convers. Biorefin*. 14(12), 12775-12783. DOI: 10.1007/s13399-022-03261-y

Carrier, M., Windt, M., Ziegler, B., Appelt, J., Saake, B., Meier, D., and Bridgwater, A. (2017). "Quantitative insights into the fast pyrolysis of extracted cellulose, hemicelluloses, and lignin," *ChemSusChem* 10, 3212-3224. DOI: 10.1002/cssc.201700984

Chen, W., Yang, H., Liu, B., Li, K., Chen, Y., Li, S., Chen, X., and Chen, H. (2014). "Effect of temperature on characteristics products derived from bamboo chips pyrolysis based on pyrolytic polygeneration," *Trans. Chin. Soc. Agric. Eng.* 30(22), 245-252. [in Chinese]

Chen, Z., Wang, M., Jiang, E., Wang, D., Zhang, K., Ren, Y., and Jiang, Y. (2018). "Pyrolysis of torrefied biomass," *Trends Biotechnol.* 36(12), 1287-1298.

Dai, Q., Wei, X., Tang, H., Li, J., and Wang, J. (2020). "Optimization of microwave assisted pyrolysis of coconut clothes by response surface method and analysis of liquid product composition," *Biomass Chemical Engineering* 54(4), 43-48. DOI:10. 3969/j.issn.1673-5854.2020.04.007 [In Chinese]

Fan, Y., Cai, Y., Li, X., Zhao W., and Yu, N. (2014). "Influence of process parameters on bio-oil yield by vacuum pyrolysis," *Chemistry and Industry of Forest Products* 34(1), 79-85. DOI: 10.3969/j.issn.0253-2417.2014.01.013 [In Chinese]

He, Z., Qian, J., Wang, Z., Yi, S., and Mu, J. (2018). "Effects of ultrasound pretreatment on eucalyptus thermal decomposition characteristics as determined by thermogravi-metric, differential scanning calorimetry, and Fourier transform infrared analysis," *ACS Omega* 3(6), 6611-6616. DOI: 10.1021/acsomega.8b00382

He, Z., Wang, Z., Qu, L., Qian, J., and Yi, S.-L. (2019). "Gaseous decomposition products from wood degradation via thermogravimetric and Fourier transform infrared analysis during thermal modification of beech and pine woods," *BioResources* 14(3), 6883-6894. DOI: 10.15376/biores.14.3.6883-6894

Keiluweit, M., Nico, P.S., Johnson, M.G., and Kleber, M. (2010). "Dynamic molecular structure of plant biomass-derived black carbon (biochar)," *Environmental Science & Technology* 44(4), 1247-1253. DOI: 10.1021/es9031419

Liu, X., Meng, W., Cheng, S., Xing, B., Zheng, Y., Ren, X., Xue, M., Zhang, C., and Xia, H. (2022). "Utilization of *Camellia oleifera* shell for production of valuable products by pyrolysis," *Arab. J. Chem.* 2022, 15(12), article 104348. DOI: 10.1016/j.arabjc.2022.104348

Liu, Q., Wang, S., Zheng, Y., Luo, Z., and Cen, K. (2008). "Mechanism study of wood lignin pyrolysis by using TG-FTIR analysis," *J. Anal. Appl. Pyrolysis* 82(1), 170-177. DOI: 10.1016/j.jaap.2008.03.007

Mehmood, T., Khan, A.U., Dandamudi, K. P. R., Deng, S., Helal, M. H., Ali, H. M., and Ahmad, Z. (2022). "Oil tea shell synthesized biochar adsorptive utilization for the nitrate removal from aqueous media," *Chemosphere* 307(3), article 136045. DOI: 10.1016/j.chemosphere.2022.136045

Meng, M., Meng, W., Cheng, S., Xing, B., Yi, G., and Zhang, C. (2022). "Effect of pyrolysis temperature on pyrolysis of *Camellia oleifera* shell," *Biomass Convers. Biorefin.* 14, 26753-26763. DOI: 10.1007/s13399-022-03317-z

Miao, Y., Kan, Y., Li, N., and Zhai, S. (2025). "Comparation of pyrolytic behaviors of brown-rotted wood and enzymatic hydrolysis lignin," *J. For. Eng.* 10(1), 60-69. [in Chinese]

Papuga, S., Savković, J., Djurdjevic, M., and Ciprioti, S. (2024). "Effect of feed mass, reactor temperature, and time on the yield of waste polypropylene pyrolysis oil produced *via* a fixed-bed reactor," *Polymers* 16(10), article 1302. DOI: 10.3390/polym16101302

Shrivastava, P., Kumar, A., Tekasakul, P., Lam, S. S., and Palamanit, A. (2021). "Comparative investigation of yield and quality of bio-oil and biochar from pyrolysis of woody and non-woody biomasses," *Energies* 2021, 14(4), article 1092. DOI: 10.3390/en14041092

Stutz, K. P., Dann D., Wambsganss, J., Scherer-Lorenzen, M., and Lang, F. (2017). "Phenolic matter from deadwood can impact forest soil properties," *Geoderma* 288, 204-212. DOI:10.1016/j.geoderma.2016.11.014

Sun, J., He, F., Pan, Y., and Zhang, Z. (2016). "Effects of pyrolysis temperature and residence time on physicochemical properties of different biochar types," *Soil & Plant Science* 67(1), 12-22. DOI: 10.1080/09064710.2016.1214745

Tang, X., Gao, W., Duan, S., Xu, J., Wang, B., and Zeng, J. (2024). "Characteristics and adsorption of methylene blue on activated carbon derived from enzyme-pretreated *Camellia oleifera* shells," *Ind. Crops Prod.* 222(1), article 119505. DOI: 10.1016/j.indcrop.2024.119505

Tong, T., Ma, Z., Chen, D., and Zhang, Q. (2014). "Pyrolysis characteristics and kinetics study of bamboo holo-cellulose using TG-FTIR," *J. Zhejiang A&F Univ.* 31(04), 495-501. DOI: 10.11833/j.issn.2095-0756.2014.04.001[In Chinese]

Xia, M., Wang, Y., Zhang, S., Zeng, Y., Liu, Y., and Ruan, R. (2021). "Research progress on comprehensive utilization of *Camellia oleifera* Abel shell," *Biomass Chem. Eng*. 55(06), 26-36. [in Chinese]

Xu, J., Zhang, S., Shi, Y., Zhang, P., Huang, D., Lin, C., and Wu, Y. (2022a). "Upgrading the wood vinegar prepared from the pyrolysis of biomass wastes by hydrothermal pretreatment," *Energy* 244(A), article 122631. DOI: 10.1016/j.energy.2021.122631

Xu, K., Jiang, Z., and Yu, Y. (2022b). "Research on VOCs release during pyrolysis of *Pterocarpus santalinus*," *China For. Prod. Ind.* 59(12), 13-19. DOI: 10.19531/j.issn1001-5299.202212003 [In Chinese]

Xu, X., and Jiang, E. (2014). "Hydrogen from wood vinegar via catalytic reforming over Ni/Ce/γ-Al2O3 catalyst," *J. Anal. Appl. Pyrolysis* 107, 1-8. DOI: 10.1016/j.jaap.2013.12.003

Yang, H., Yan, R., Chen, H., Lee, D. H., and Zheng, C. (2007). "Characteristics of hemicellulose, cellulose and lignin pyrolysis," *Fuel* 86(12-13), 1781-1788. DOI: 10.1016/j.fuel.2006.12.013

Yuan, Y., Kong, Q., Zheng, Y., Zheng, H., Liu, Y., Cheng, Y., Zhang, X., Li, Z., You, X., and Li, Y. (2022). "Co-application of biochar and pyroligneous acid improved peanut production and nutritional quality in a coastal soil," *Environ. Technol. Innov.* 28, article 102886. DOI: 10.1016/j.eti.2022.102886

Yang, Z., Fu, L., and Fan, F. (2019). "Thermal characteristics and kinetics of waste *Camellia oleifera* shells by TG-GC/MS," *ACS Omega* 4(6), 10370-10375. DOI: 10.1021/acsomega.9b01013

Zhang, L., Gao, J., Wang, T., Hao, T., Lu, Y., Hu, Y., Wang, X., He, Z., Wang, Z., and Yi, S. (2025). "Catalytic pyrolysis characteristics of potassium chloride on ash branch wood and its kinetic study," *Forests* 16(1), article 57. DOI: 10.3390/f16010057

Zhang, L., He, Y., Zhu, Y., Liu, Y., and Wang, X. (2018). "*Camellia oleifera* shell as an alternative feedstock for furfural production using a high surface acidity solid acid catalyst," *Bioresource Technol.* 249, 536-541. DOI: 10.1016/j.biortech.2017.10.061

Zhang, M., Jiang, Z., and Ma, Z. (2018). "VOC emission during the pyrolysis of poplar," *China For. Prod. Ind.* 2018, 45(12), 29-34. [in Chinese]

Zhang, W., Li, Y., and Cai, Z. (2015). "The development of wood pyrolysis technology," *China For. Prod. Ind.* 42(12), 8-11. [in Chinese]

Zhang, Y., He, B., Xue, L., Chua, D. M., and Mu, J. (2016). "Influence of a urea-formaldehyde resin adhesive on pyrolysis characteristics and volatiles emission of poplar particleboard," *RSC Adv.* 6(16), 12850-12861. DOI: 10.1039/c5ra18068f

Zheng, H., Lv, D., Xu, F., and Chen, X. (2024). "Research progress on preparation and application of activated carbon from oil tea shells," *Mod. Chem. Res.* 22, 12-14. [in Chinese]

Article submitted: April 1, 2025; Peer review completed: July 11, 2025; Revised version received: October 13, 2025; Accepted: October 16, 2025; Published: October 29, 2025.
DOI: 10.15376/biores.20.4.10893-10905